Plasmonically-enhanced CRISPR/Cas13a-based Bioassay for Amplification-free Detection of Cancer-associated RNA

Lin Liu[1, &], Zheyu Wang[1, &], Yixuan Wang[1], Jingyi Luan[1], Jeremiah J. Morrissey[2, 3], Rajesh R. Naik[4], Srikanth Singamaneni[1, 3, *]*

[1]Department of Mechanical Engineering and Materials Science, Institute of Materials Science and Engineering, Washington University in St. Louis, St Louis, MO, 63130, USA.

[2]Department of Anesthesiology, Washington University in St. Louis, St. Louis, MO, 63110, USA

[3]Siteman Cancer Center, Washington University School of Medicine, St. Louis, MO, 63110, USA

[4]711 Human Performance Wing, Air Force Research Laboratory, Wright Patterson Air Force Base, Dayton, OH, 45433, USA

& These authors contributed equally

*To whom correspondence should be addressed: singamaneni@wustl.edu (SS) and rajesh.naik@us.af.mil (RRN)

Abstract

Novel methods that enable sensitive, accurate and rapid detection of RNA would not only benefit fundamental biological studies but also serve as diagnostic tools for various pathological conditions, including bacterial and viral infections and cancer. Although highly sensitive, existing methods for RNA detection involve long turn-around time and extensive capital equipment. Here, we demonstrate an ultrasensitive and amplification-free RNA quantification method by integrating CRISPR-Cas13a system with an ultrabright fluorescent nanolabel, plasmonic fluor. This plasmonically enhanced CRISPR-powered assay exhibited nearly 1000-fold lower limit-of-detection compared to conventional assay relying on enzymatic reporters. Using a xenograft tumor mouse model, we demonstrated that this novel bioassay can be used for ultrasensitive and quantitative monitoring of cancer biomarker (lncRNA H19). The novel biodetection approach described here provides a rapid, ultrasensitive and amplification-free strategy that can be broadly employed for detection of various RNA biomarkers, even in resource-limited settings.

Key words: CRISPR-Cas13a; plasmon-enhanced fluorescence; RNA detection; gold nanorods; nanolabels.

1. Main

RNAs, as the genetic messengers, play essential regulatory roles in the development of cells and tissues as well as the progression of disease.[1] Simple and effective methods that enable highly sensitive detection and quantification of RNAs will advance our understanding of gene expression profiles and elucidate their role in cellular function and dysfunction.[2-5] There is a dire need for ultrasensitive and low-cost RNA diagnostics since timely and accurate detection of RNA allows effective monitoring and control of infectious disease outbreaks and early detection of other pathological conditions, including cancer.

Quantitative reverse transcription polymerase chain reaction (qRT-PCR) is the current gold standard for RNA detection. Despite its superior sensitivity compared to other existing methods, reliance on bulky and expensive equipment, laborious sample preparation and time-consuming process, precludes its application in resource-limited settings and for screening large populations.[6-7] Other RNA detection techniques, including microarray and ribonucleic acid fluorescent in situ hybridization (RNA FISH), come with their own limitations in signal specificity, sensitivity and stability.[8-12] Therefore, an ultrasensitive, low cost, easy-to-use and rapid RNA quantification technique will overcome these limitations and enable large-scale screening of infectious diseases and other diseases in resource-limited settings.

Over the last few years, clustered regularly interspaced short palindromic repeats (CRISPR) - associated (Cas) protein system has emerged as a highly efficient and powerful gene editing tool and has been extensively harnessed by a broad scientific community for *in vivo* gene engineering and *ex vivo* biodetection.[13-18] The elegance of CRISPR-Cas-based biodetection lies in the combination of programmable recognition and target-dependent actuation. The specificity in the detection of target RNA is achieved by designing the CRISPR RNA (crRNA) to be complementary to the target RNA (trRNA) sequence. Upon recognition and binding of the target RNA to the crRNA, the single strand RNA (ssRNA) cleavage ability of the CRISPR/Cas13a is activated. The recognition ability allows CRISPR/Cas13a to discriminate even single-base mismatch, significantly improves the sensing accuracy compared with conventional methods such as qRT-PCR.[19-20] However, the conventional approach of CRISPR-Cas-based biodetection involves reporter RNA (reRNA) labeled with a Förster resonance energy transfer (FRET) pair, where the cleavage of reRNA results in the activation of the fluorescence signal.[13, 17-18] The weak

fluorescence signals associated with the conventional fluorophores inevitably require a pre-amplification process, such as recombinase polymerase amplification, which is error-prone and requires elaborate design of primers, thus mostly utilized as a qualitative method. [6]

The weak fluorescence signal and the associated poor signal-to-noise ratio are the major challenges to fluorescence-based bioassays, severely hampering the sensitivity of these assays. Nanostructures, capable of enhancing the brightness of individual fluorophores[21-22], increasing the packing density of fluorescent molecules[23-24], or reducing the background fluorescence[25], have been employed as nanolabels in the immunoassay. Ultrabright fluorescent nanostructures, which can be employed in a simple and effective means to amplify the fluorescence signal without altering the established assay procedures, are highly attractive for realizing highly sensitive bioassays. Integration of such nanolabel-based signal amplification with the remarkable specificity and the inherent signal amplification ability of CRISPR/Cas system is highly attractive to improve the sensitivity of RNA detection.

In this work, we demonstrate a plasmonically-enhanced fluoroimmunoassay integrated with CRISPR-Cas system for ultrasensitive and quantitative measurement of RNA. In contrast to conventional approach, we employed plasmonic-fluor as an ultrabright and highly specific fluorescent nanolabel, instead of conventional fluorophores, to improve the sensitivity. Plasmonic fluor exhibits up to 6700-fold brighter signal compared to the corresponding single fluorophore and has been demonstrated to improve the sensitivity up to three orders of magnitude for a variety of bioanalytical assays, including fluorescence linked immunosorbent assay (FLISA), immunomicroarrays, multiplexed bead-based fluoroimmunoassays and flow cytometry.[9] Here, we demonstrate that integration of plasmonically-enhanced fluoroimmunoassay with CRISPR-Cas system results in an ultrasensitive, rapid and easy-to-use RNA quantification method that can be employed for the detection and quantification of clinically-relevant RNA in biological samples in biomedical research and clinical diagnosis (**Figure 1**).

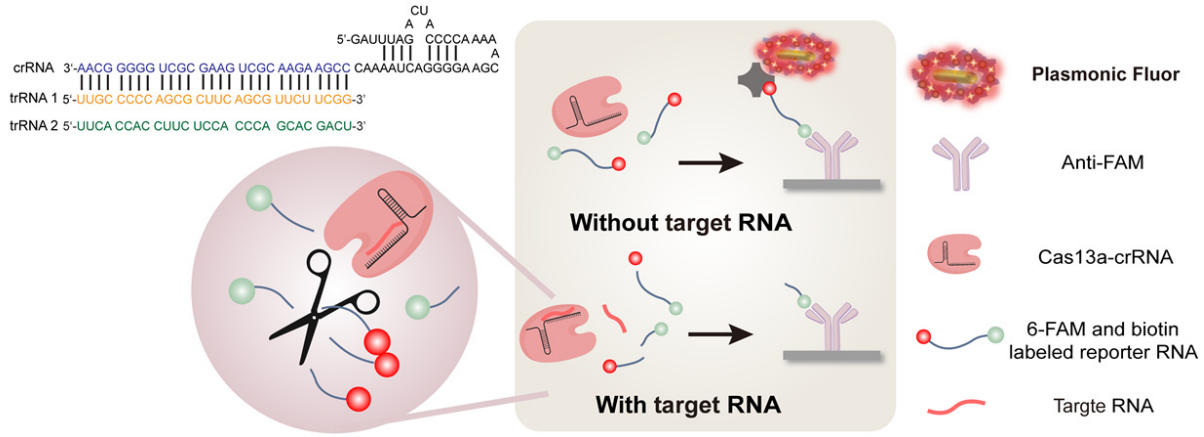

Figure 1. Schematic of CRISPR-powered plasmonically enhanced amplification-free assay. Initially, crRNA recognizes and binds with target RNA (trRNA), activating Cas13a to cleave the nearby reporter RNA (reRNA, single-stranded RNA with 6-FAM and biotin label on either ends). Subsequently, this reaction solution is incubated on anti-FAM coated microtiter plate, followed by washing and exposure to plasmonic-fluor, an ultrabright nanolabel. Only the uncleaved reRNA will specifically bind to plasmonic-fluor, and, therefore, higher signal intensity indicates less amount of trRNA present in the original sample.

To evaluate the feasibility of using plasmonic-fluor as an ultrabright fluorescence reporter, we set out to determine and compare the brightness of plasmonic-fluor with conventional fluorophores. Plasmonic-fluor-Cy7.5 used in this work is comprised of Au@Ag nanorods as a plasmonic nanoantenna and is coupled with fluorophores (Cy7.5), bovine serum albumin and streptavidin as biorecognition element (Figure 2A, 2B). The microtiter plate coated with BSA-biotin was exposed to plasmonic-fluor-Cy7.5 and streptavidin-Cy7.5. The fluorescence intensity corresponding to plasmonic-fluor was found to be nearly 1100-fold higher compared to that of streptavidin-Cy7.5. (Figure 2C, Figure S1).

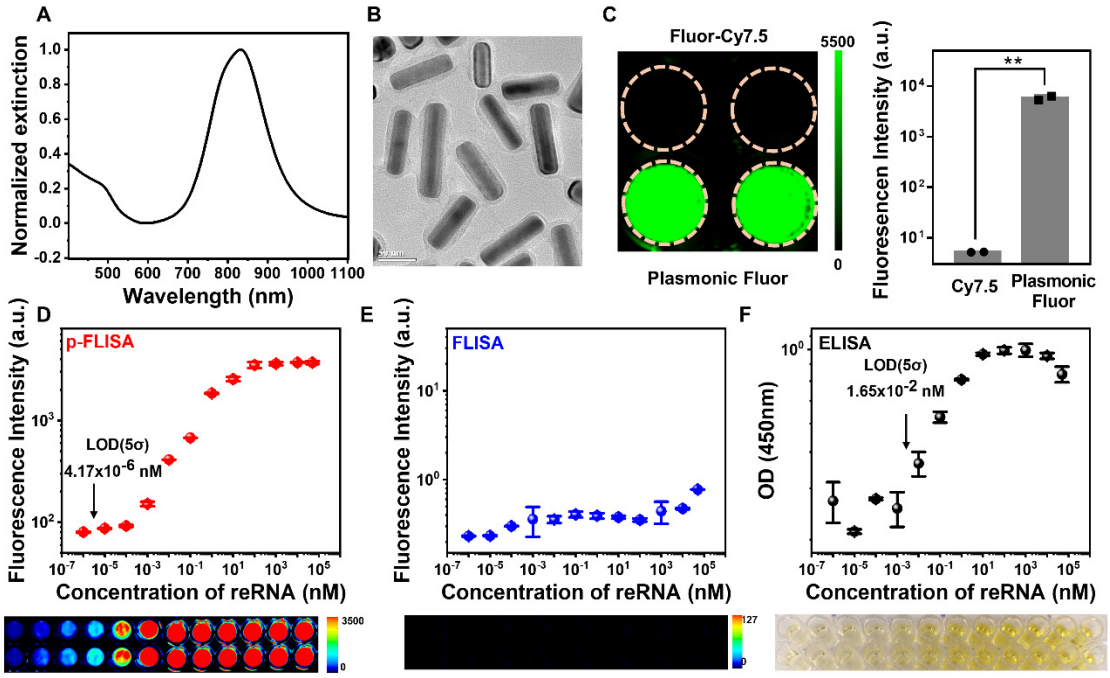

Figure 2 Plasmoncally enhanced RNA assay. **A)** Vis–NIR extinction spectra of plasmonic-fluor, showing longitudinal plasmonic extinction band at 800nm; **B)** TEM image plasmonic-fluor–Cy7.5; **C)** Fluorescence intensity map and histogram corresponding to conventional fluor and plasmonic-fluor showing nearly 1100-fold brighter fluorescence intensity of plasmonic-fluor compared to conventional fluor. Error bars, s.d. (n = 2 independent tests). Data statistically significant ** $P < 0.01$ by two-tailed unpaired t-test with Welch's correction. **D)-F)** Standard curve obtained by incubating anti-FAM antibody coated plates with serially diluted reRNA followed by incubation with streptavidin-plasmonic-fluor **D)**, streptavidin-Cy7.5 **E)**, and streptavidin-HRP **F)**, respectively. Technical replicates with n=2, and data is presented as mean ± s.d. Within the concentration range tested, conventional FLISA did not exhibit dose-dependent standard curve. Compared with ELISA, p-FLISA exhibited 4 orders lower LOD. Error bars, s.d. (n = 3 independent tests).

To investigate the applicability of plasmonic fluor as an ultrabright fluorescence label in CRISPR-powered fluoroimmunoassay, ssRNA labelled with 6-fluorescein amidite (6-FAM) and biotin was employed as reRNA in CRISPR-Cas13a cleavage process. reRNA also acts as the analyte in the downstream plasmonic-fluor enhanced fluoroimmunoassay. Conventional fluorophore-linked immunosorbent assay (FLISA) involves the recognition and capture of reRNA (following the exposure to CRISPR-Cas13a for possible enzymatic cleavage in the presence of target RNA) by anti-FAM antibody followed by exposure to fluorophore-labelled streptavidin. In contrast, plasmonic fluor-linked immunosorbent assay (p-FLISA) involves the use of plasmonic fluor,

instead of conventional fluorophores or enzymes, as the signal reporter. To determine the improvement in sensitivity and limit-of-detection rendered by plasmonic fluor, serial dilutions of reRNA with known concentration (10^{-7} nM to 10^{4} nM) were used as standards to simulate different levels of enzymatic cleavage, which in turn corresponds to different concentrations of target RNA. At the highest reRNA concentration (10^{7} nM), the fluorescence signal intensity obtained using plasmonic-fluor was nearly 3700-fold higher compared to that obtained with conventional fluorophore. The LOD of p-FLISA was found to be 4.17 fM, while the fluorescence signal obtained for different concentrations of reRNA in conventional FLISA are low and close to that of the blank (Figure 2D, 2E). Furthermore, ELISA exhibited weak colorimetric signal and a large standard deviation at low concentration (Figure 2F). The LOD of ELISA was found to be ~16.5 pM, which is nearly 4000-fold higher compared to that of p-FLISA.

To determine the sensitivity and LOD (defined as mean+3σ of the blank) of p-FLISA in CRISPR-powered RNA detection, we employed serial diluted RNA, 5' UUGC CCCC AGCG CUUC AGCG UUCU UCGG A 3' (referred to as trRNA-1 henceforth), as standards and complementary guide RNA 3'AACG GGGG UCGC GAAG UCGC AAGA AGCC CAAA AUCA GGGG AAGC UAUA ACCC ACC 5' as guide RNA (referred to as crRNA-1 henceforth) (Figure 1). CRISPR-Cas13a was expressed and purified according to a previous report[26] and validated by a single band at 150 kDa on SDS-PAGE gel (Figure S2). Serial dilution of trRNA-1 were incubated with Cas13a, crRNA-1 and reRNA, activating CRISPR enzymes, and leading to the cleavage of the reRNA. The mixture was incubated at 37°C for 2 hours to allow enzymatic cleavage. Subsequently, this solution was added to anti-FAM coated microtiter plate for 1 hour where both cleaved and uncleaved reRNAs are captured by anti-FAM antibody. Finally, addition of streptavidin-bearing plasmonic-fluors to the microtiter wells resulted in the binding of the plasmonic-fluors to the uncleaved reRNA. As expected, an increase in the concentration of the trRNA-1 resulted in a progressive decrease in fluorescence intensity, as more target RNA leads to more activated Cas13a/crRNA-1 complex and less plasmonic-fluor binding on the plate. We further improved the sensitivity of the assay by optimizing the concentration of reRNA. Serially diluted trRNA-1 was incubated with Cas13a, crRNA-1 and different concentrations of reRNA before performing the downstream p-FLISA. The LOD of CRISPR powered p-FLISA was found to be 8.76 nM, 5.18 nM, 0.011 nM, 0.82 nM and 1.13 nM for reRNA concentrations at 40 nM, 4 nM, 0.4 nM, 0.04 nM and 0.004 nM, respectively (Figure 3A-E). At higher concentrations of reRNA, the chance of

cleavage of reRNA are greater, while the percentage of cleaved reRNA is lower resulting in lower sensitivity of the assay. At lower concentrations of reRNA, the chances of cleavage are lower but the percentage of cleaved reRNA is higher. Overall, we found the optimal concentration of reRNA to be 0.4 nM for attaining the highest sensitivity. Other factors including the cleavage time and plasmonic-fluor concentration also influence the sensitivity of this assay. To investigate the optimal cleavage time, we incubated the reaction mixture comprised of Cas13a, tr RNA, crRNA, and reRNA for 0.5, 1 and 2 hours. We found that the longer time cleavage time resulted in higher sensitivity (Figure S7). Similarly, the effect of plasmonic-fluor concentration was also systematically studied. We noted that ext 0.5 provided the highest sensitivity (Figure S8).

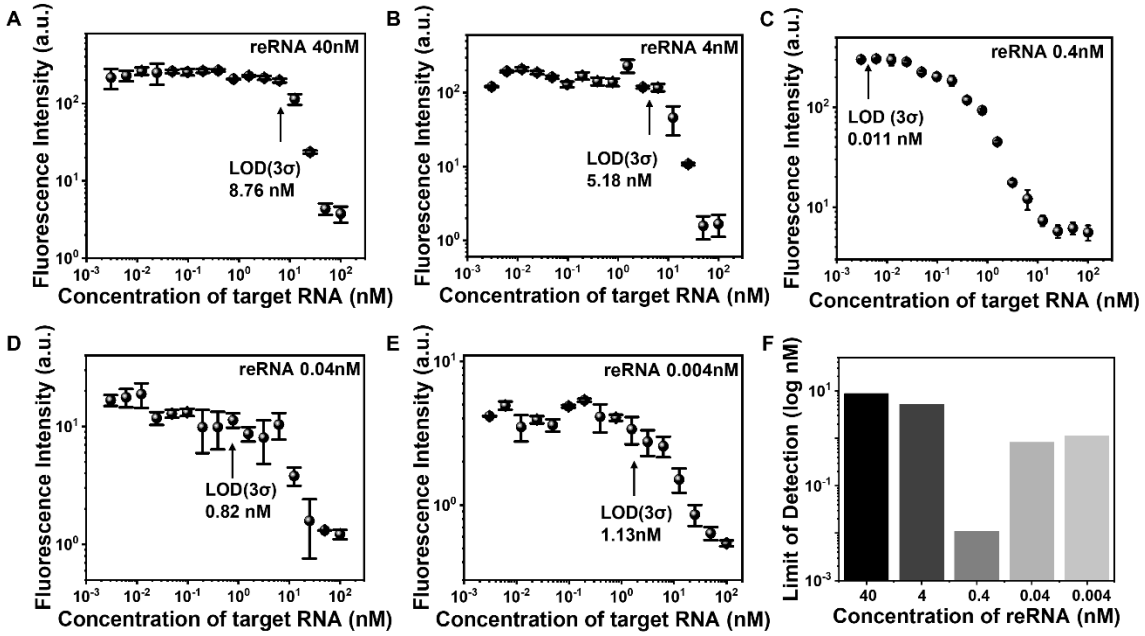

Figure 3 Effect of reRNA concentration on LOD A)-E) Plots showing target RNA dose-dependent response of CRISPR-powered assay using different reRNA concentration (from 40 nM to 0.004 nM). The LOD decreased from 8.76 nM to 11 pM with a decrease in reRNA from 40 nM to 0.4 nM. Technical replicates with n=2, and data is presented as mean $\pm$ s.d. **F)** Plot showing log (LOD) of CRISPR-powered assay with varying concentrations of reRNA.

To investigate the specificity of p-FLISA based CRISPR-powered RNA detection, we employed complementary RNA sequence trRNA-H19 as the target RNA and three synthetic RNA sequences with 1, 3 and 22 nucleobases mismatch as the off-target RNAs (Figure S3). Ideally, the absence of

complementarity between the crRNA-1 and mismatched trRNA is expected to result in no activation of Cas13a, thereby no cleavage of the by standing reRNA. Same concentration (10 nM) of trRNA-H19 (target) and mismatched trRNAs (off-target) were introduced separately into the reaction solution comprised by Cas13a, crRNA-1 and reRNA, and subsequently subjected to p-FLISA. Fluorescence intensity obtained in the presence of off-target trRNA-with more than two nucleobases mismatch is found to be almost identical to that of the blank (*i.e.* no target RNA), and the trRNA with single nucleobase mismatch exhibited signal intensity of more than 90% of the blank. On the other hand, fluorescence intensity obtained in the presence of trRNA-H19 is ~10% of the blank, suggesting the specific recognition and cleavage of reRNA by Cas13a/crRNA-1 complex (Figure S3). These results indicate the high specificity of plasmonically-enhanced CRISPR-powered assay.

Long noncoding RNAs (lncRNAs), composed of more than 200 nucleotides, are single-stranded RNAs (ssRNAs) without evident protein coding function. As a class of regulatory non-coding RNA, lncRNAs spatially regulate the gene expression in the cells by serving as guides for DNA methylation, scaffolds for ribonucleoprotein complex formation, and decoys for transcription factors.[27] In recent studies, lncRNAs have been recognized as biomarkers for multiple diseases including cancer, lung diseases, cardiocerebrovascular diseases, and immune diseases.[27-35] More importantly, compared to mRNA, the expression of lncRNAs is more tissue-specific, which could help tracing cancer metastasis to its origins.[36] For instance, studies have shown that long non-coding RNA H19 (lncRNA H19) is a reliable cancer-associated biomarker and its expression level is upregulated in various types of cancers, including ovarian cancer, breast cancer, gastric cancer, and colorectal cancer.[32, 37-39] Herein, we set out to demonstrate the quantitative measurement of this clinically-relevant RNA, lncRNA H19, within biological samples using the plasmonically-enhanced CRISPR-powered assay.

First, to determine the sensitivity of CRISPR-powered p-FLISAlncRNA was found to be nearly 6 pM, while samples tested by conventional FLISA exhibited nearly identical fluorescent intensity for all dilutions (Figure 4A, 4B). The LOD of nucleic acid ELISA was found to be nearly 4 nM, which is nearly 1000-fold higher compared to that obtained using p-FLISA (Figure 4B).

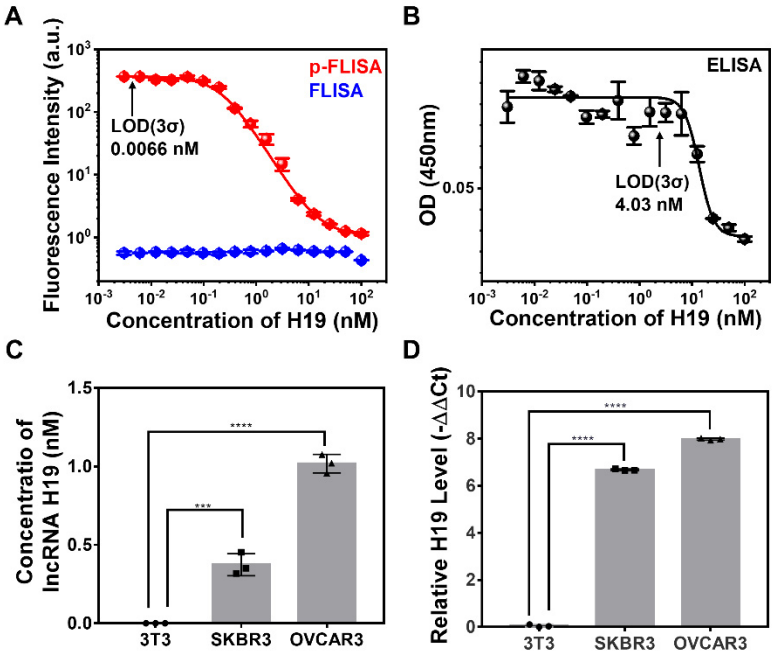

Figure 4 CRISPR-powered RNA assay for testing cell lysate samples A)&B) Plots showing target RNA lncH19 dose-dependent response in CRISPR-powered p-FLISA assay **A)**, CRISPR-powered conventional FLISA assay **A)**, and CRISPR-powered ELISA assay **B).** Technical replicates with n=2, and data is presented as mean ± s.d. The LOD of CRISPR-powered p-FLISA is 610-fold lower than CRISPR-powered ELISA. **C)** Plot showing the concentration of H19 within 3T3, SK-BR-3, and OVCAR-3 cell lines obtained from CRISPR-powered p-FLISA. Error bars, s.d. (n = 3 independent tests). **D)** Plot showing the relative concentration of H19 expressed by -ΔΔCt within 3T3, SK-BR-3, and OVCAR-3 cell lines. Error bars, s.d. (n = 3 independent tests). Data statistically significant. ****$P < 0.0001$, *** P< 0.001 by Student t test.

We explored the use of our method in testing biological samples. method in testing biological samples. We measured expression level of lncRNA H19 in human ovarian cancer cells (OVCAR-3), and human breast cancer cells (SK-BR-3). Total RNA was first extracted from cell lysate using a commercial RNA purification kit. The purified total RNA solution was diluted to achieve a concentration of 250 ng/ml before mixing with Cas13a, reRNA and crRNA specific to lncRNA H19. We attained a standard curve by spiking known concentrations of lncRNA H19 in total RNA (250 ng/ml) extracted from 3T3 cells (Figure S4). Total RNA isolated from 3T3 cells are known to have negligible amount of lncRNA H19. Based on this standard curve, the concentration of lncRNA H19 was found to be 0.37 nM in RNA solution from SK-BR-3 cells and 1.02 nM RNA solution from OVCAR-3 cells (Figure 4C). To validate the measurement accuracy, we performed

standard qRT-PCR of identical samples that provided relative concentration of lncRNA H19. The results of qRT-PCR exhibited good qualitative correlation with those measured by CRISPR-powered p-FLISA, where the total RNA extracted from OVCAR-3 exhibited higher level of lncRNA H19 compared to that from SK-BR-3 while 3T3 cells corresponded to negligible amount of lncRNA H19 (Figure 4C, 4D).

Measurement of cancer biomarkers in standard tissue biopsy allows the diagnosis of primary tumors or determining the stage of metastatic lesion.[37, 40-42] To explore the feasibility of using CRISPR-powered p-FLISA for H19 detection in biopsy specimen, we established a human ovarian cancer xenograft mouse model. Owing to the immunodeficiency, the athymic nude mice allow the natural growth of human cancer cell lines *in vivo* with similar behavior, including proliferation, migration and inducing angiogenesis, resulting in the tumor microenvironment with upregulated level of oncogenic genes, such as lncRNA H19. [38, 43]

Nude mice were subcutaneously injected with human epithelial ovarian cancer cells (OVCAR-3) into the inguinal region (Figure 5A, Figure S5). Tumors were surgically isolated and weighed during the 6th week, followed by extraction of total RNA and analysis by CRISPR-powered p-FLISA (Figure 5B). On the basis of standard curve, the concentrations of lncRNA H19 were found to be 45.3 nM, 38.9 nM, 47.0 nM, 57.5 nM in extracted RNA solution from each mouse (Figure 5C). The concentration of lncRNA H19 within the same tissue biopsy tested by qRT-PCR also revealed a good qualitative correlation with those evaluated by CRISPR-powered p-FLISA ($r^2_{CRISPR\text{-}PCR}$=0.96) (Figure S6). These results indicate the high accuracy of this novel assay in measuring the concentration of target in complex biospecimen. Significantly, the concentration of lncRNA H19 correlated well with the tumor weight ($r^2_{CRISPR\text{-}Weight}$=0.90). As an oncogenic gene, lncRNA H19, is suggested to be highly correlated to the clinical symptoms and its concentration is known to increase with the size of the tumor (Figure 5D).

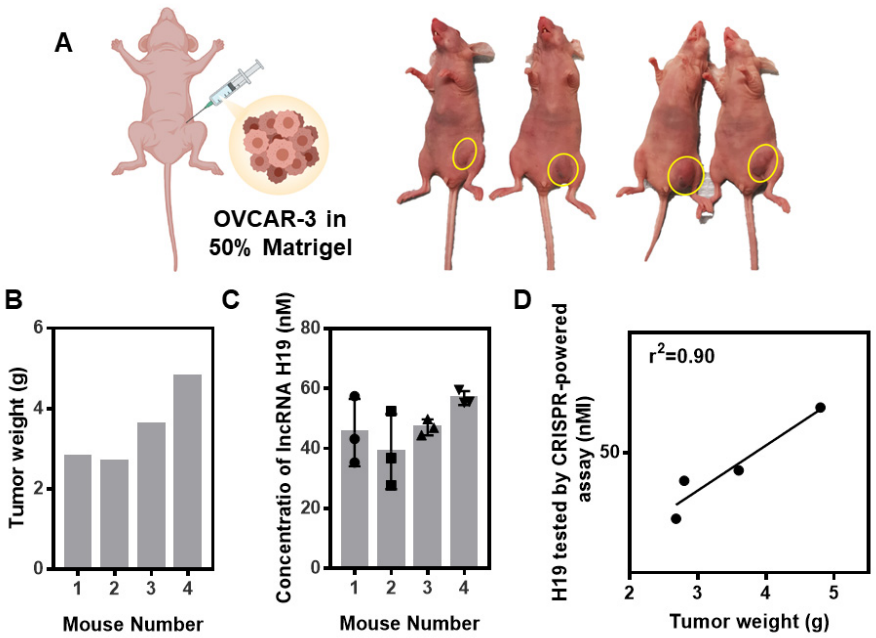

Figure 5 CRISPR-powered RNA assay of OVCAR-3 xenograft model A) Schematic of OVCAR-3 xenograft model. **B)** The weight of the tumor tissue in different mice. **C)** The concentration of H19 in tumor tissue obtained using CRISPR-powered p-FLISA assay. Error bars, s.d. (n = 3 independent tests). **D)** Plot showing the correlation between concentration of H19 and weight of the tumor tissue. r^2=0.90 Tested by Pearson r.

2. Conclusion

In summary, we have demonstrated an amplification-free, specific, and ultrasensitive RNA detection and quantification technology based on CRISPR-Cas13a coupled with plasmonically-enhanced fluoroimmunoassy. Plasmonic-fluor, which serves as an ultrabright fluorescence reporter, significantly improved the sensitivity of the downstream immunoassay. The LOD of the plasmon-enhanced detection method is nearly three orders of magnitude better compared with the assays relying on conventional enzymatic or fluorophore reporters. With similar accuracy as qRT-PCR, the CRISPR-powered nucleic acid p-FLISA technique is highly attractive for detection and quantification of clinically-relevant RNA in cell lysates and tissue biopsies without any pre-amplification process. Owing to its high sensitivity and specificity and simplicity, plasmon-enhanced CRISPR-powered assay demonstrated here can be highly attractive for detection of target RNA in point-of-care (POC) and resource-limited settings.

3. Methods & Materials

Plasmonic-fluor, synthesized according to procedure described previously, was purchased from Auragent Bioscience, LLC.[9]

3.1 Recombinant expression and purification of LwaCas13a

LwaCas13a was expressed and purified according to a protocol reported previously.[26] Briefly, the pC013-Twinstrep-SUMO-huLwCas13a (Addgene NO.90097) was transformed into Rosetta™ 2(DE3)pLysS Singles™ Competent Cells (Sigma-Aldrich, 71401-3) followed by inducing LwaCas13a expression with 500 μM IPTG (Sigma-Aldrich, I5502-1G). Cells were harvested by centrifugation at 10,000 g for 15 min at 4 °C and stored at −80°C.

3.2 Purification of LwaCas13a

All purification steps were performed at 4°C. Samples from different purification steps were verified by SDS-PAGE analyses shown in Figure S1. Cell pellets were resuspended and ruptured by sonication (Qsonica,Q700 Sonicators). Lysate was spun down for 1 h at 10,000 g and the supernatant was filtered through a Stericup 0.22 μm filter (EMD Millipore). Filtered supernatant was then applied to StrepTactin Superflow Plus resin (Qiagen, 30004), followed by washing to remove other major impurities before resuspension in 250 units of SUMO protease for overnight incubation (Sigma-Aldrich, SAE0067-2500UN).

To remove remaining impurities including SUMO proteases and nucleases, enzyme was further purified via fast protein liquid chromatography (FPLC) (AKTA PURE, GE Healthcare Life Sciences). The fraction solution was tested by SDS-PAGE and fractions containing highly purified LwaCas13a were buffer exchanged to storage buffer (600 mM NaCl, 50 mM Tris-HCl, pH 7.5, 5% glycerol, 2 mM DTT) before being aliquoting and storing at -80°C for further use.

3.3 Cell culture

OVCAR3 (human ovarian carcinoma cell line), SK-BR-3 (human epithelial breast cancer cell line) and 3T3 were purchased from ATCC (American Type Culture Collection, Manassas, USA). 3T3 and SK-BR-3 cells were cultured in Dulbecco's Modified Eagle Medium (High Glucose) supplemented with 10% fetal calf serum. OVCAR3 cells were cultured in RPIM 1640 medium supplemented with 1% L-glutamine, 1% fetal insulin and 10% fetal calf serum. All cells were

grown in 75 cm^2 tissue culture flasks in a water jacket incubator at 37°C, 5% CO_2 incubator and 95% humidity.

3.4 OVCAR3 xenograft tumor model

All procedures have been approved by the Institutional Animal Care and Use Committee (IACUC) at Washington University in St. Louis (Animal protocol number: 20180107). Female homozygous nude (*Foxn1^{nu}/Foxn1^{nu}*) mice were obtained from Jackson Lab (stock number 007850). Mice were housed in the specific pathogen-free housing facility at a constant temperature (21 - 23 °C) and humidity (45-50%) on 12-hour light-dark cycle (lights on 07:00-19:00), with food and water available ad libitum throughout the study. Four to five weeks old nude (*Foxn1^{nu}/Foxn1^{nu}*) mice were subcutaneously inoculated with 10^6 OVCAR3 cells in 100 µl 50% Matrigel (USA, Corning). Mice bearing tumor were observed and their tumor length, width, and height was recorded every week. During sixth week, mice were sacrificed and the xenograft tumor tissues were harvested for RNA extraction.

3.5 Extraction of RNA and RT-qPCR analysis

RNA from cell lines and isolated tumor tissues were extracted by Trizol (Invitrogen Calsbad, USA) and Purelink RNA mini Kit (Invitrogen, Calsbad, USA) following the instructions provided by the vendor. The obtained RNA was quantified by Nanodrop (Thermo Scientific, NanoDrop 2000).

For the detection of IncH19, a two-step RT-PCR was employed. cDNA was first synthesized using PrimeScript RT Master Mix kits (Takara, 036A) following manufacturer's protocol. Subsequently, the real-time PCR of IncH19 were performed in pentaplicates using Bio-Rad CFX384 qPCR instrument (Bio-Rad, Hercules, CA) with TB Green® Premix Ex Taq™ (Takara, RR420L). Primers were designed against IncH19 and acquired from Integrated DNA Technologies (IDT) (primer sequences shown in Supporting Table1). The IncH19 levels were normalized with respect to a stable internal reference gene, GAPDH. Relative fold change between expression of target genes in experimental groups were calculated by -ΔΔCt method. This method assumes that the amplification efficiency of tested gene lncH19 is identical to that of the reference gene (GAPDH) in control sample (3T3 cell line.) First, the difference between the Ct values (ΔCt) of lncRNA H19 and GAPDH was calculated for 3T3 and experimental groups (OVCAR-3, SK-BR3, Mouse1-4). Then, the difference in the ΔCt values between the experimental groups and 3T3 ΔΔCt are calculated.

3.6 Preparation of crRNA

lncH19 RNA sequence was obtained from NONCODE (http://www.noncode.org/) and its targeting sequence for CRISPR-Cas13a assay was predicted by CRISPR-RT website (http://bioinfolab.miamioh.edu/CRISPR-RT/interface/C2c2.php). Constructs were ordered as DNA from IDT appended with a spacer sequence (5'GAUUUAGACUACCCC AAAAACGAAGGGGACUAAAAC) and a T7 promoter sequence (sequence shown in Supporting Table 2). For in vitro synthesis of crRNA, crRNA DNA was annealed to a short T7 primer and incubated with T7 polymerase overnight at 37°C using the HiScribe T7 Quick High Yield RNA Synthesis kit (E2050S, New England Biolabs) following manufacturer's protocol. Obtained crRNAs were purified using Monarch® RNA Cleanup Kit (50 µg) (T2040S-10preps, New England Biolabs) and diluted to 10 ng/µl before storage in -80 °C.

3.7 Plasmonically enhanced, CRISPR-powered RNA immunoassay

All steps were performed under DNase and RNase free condition. For targeting and actuation of CRISPR-Cas13a, the cleavage process was performed in 1.5 ml tube containing Cas13a reaction mixture solution: 62.5 µg/ml purified Cas13a, 10 ng/µl crRNA, 0.4 nM reRNA (final concentration), 4 U/µl murine RNase inhibitor (M0314L, New England Biolabs) and varying amounts of target RNA or isolated RNA from cells/tissues in nuclease-free buffer including 20 mM HEPES buffer (Fisher Scientific, BP299100) and 9 mM $MgCl_2$ (Thermo Fisher, AM9530). The reaction was allowed to proceed for 2 hours in an incubator at 37 °C before being introduced to pre-functionalized plate.

The standard microtiter plates were functionalized with anti-FAM antibody (0.5 µg/ml in PBS, Thermo Fisher, 701078) through overnight incubation at room temperature followed by blocking with 1X PBS containing 1% BSA. After three times washing with PBST (1X PBS, 0.05% Tween-20), 100 µl of Cas13a reaction mixture was added into different wells and the plate was incubated for 1 hour at room temperature. The plate was subsequently washed and incubated with plasmonic-fluor (extinction 0.5) for 30 minutes. The plate was imaged using LI-COR CLx fluorescence imager with the following scanning parameters: laser power ~L2; resolution 21 µm; channel 800; height 4 mm. The detailed assay protocol was shown in Supporting Table 3.

3.8 Statistical Analysis

The statistical analysis was performed with GraphPad Prism 6 and all values were expressed as mean ± s.d. For testing the statistical difference between two groups, an unpaired two-tailed t-test was used. Statistical significance of the data was calculated at 95% ($P < 0.05$) confidence intervals. We employed four-parameter logistic or polynomial fit to calculate the standard curves of bioassays. The LOD is defined as the analyte concentration corresponding to the mean fluorescence intensity of blank plus three times of its standard deviation (mean - 3σ). Technical replicates with n=2. Origin 2016 was employed for calculating the LOD.

Supporting Information

Supporting Information is available from the Wiley Online Library or from the author.

Acknowledgements

We acknowledge support from National Institutes of Health (R21CA236652, R01DE027098 and R01CA141521) and National Science Foundation (CBET-1900277, CBET-2027145). We also acknowledge support from the Air Force Research Laboratory. The authors thank Prof. Rohit Pappu and Dr. Matthew King for helping with Cas13a protein purification. The authors also thank Nano Research Facility (NRF) and Institute of Materials Science and Engineering (IMSE) at Washington University for providing access to electron microscopy facilities

Competing interests

The authors declare the following competing financial interest(s): J.L., J.J.M., and S.S. are inventors on provisional patent related to this technology and the technology has been licensed by the Office of Technology Management at Washington University in St. Louis to Auragent Bioscience LLC, which is developing plasmonic-fluor products. J.L., J.J.M., and S.S. are co-founders/shareholders of Auragent Bioscience LLC. These potential conflicts of interest have been disclosed and are being managed by Washington University in St. Louis.

References

1. Higgs, P. G.; Lehman, N., The RNA World: molecular cooperation at the origins of life. *Nature reviews. Genetics* **2015,** *16* (1), 7-17.
2. Helm, M.; Motorin, Y., Detecting RNA modifications in the epitranscriptome: predict and validate. *Nature reviews. Genetics* **2017,** *18* (5), 275-291.
3. Li, Y.; Zheng, Q.; Bao, C.; Li, S.; Guo, W.; Zhao, J.; Chen, D.; Gu, J.; He, X.; Huang, S., Circular RNA is enriched and stable in exosomes: a promising biomarker for cancer diagnosis. *Cell research* **2015,** *25* (8), 981-4.
4. Lu, D.; Thum, T., RNA-based diagnostic and therapeutic strategies for cardiovascular disease. *Nature reviews. Cardiology* **2019,** *16* (11), 661-674.
5. Voigt, F.; Gerbracht, J. V.; Boehm, V.; Horvathova, I.; Eglinger, J.; Chao, J. A.; Gehring, N. H., Detection and quantification of RNA decay intermediates using XRN1-resistant reporter transcripts. *Nat Protoc* **2019,** *14* (5), 1603-1633.
6. Bleve, G.; Rizzotti, L.; Dellaglio, F.; Torriani, S., Development of reverse transcription (RT)-PCR and real-time RT-PCR assays for rapid detection and quantification of viable yeasts and molds contaminating yogurts and pasteurized food products. *Appl Environ Microbiol* **2003,** *69* (7), 4116-22.
7. Smith, C. J.; Osborn, A. M., Advantages and limitations of quantitative PCR (Q-PCR)-based approaches in microbial ecology. *FEMS Microbiol Ecol* **2009,** *67* (1), 6-20.
8. Clancy, E.; Burke, M.; Arabkari, V.; Barry, T.; Kelly, H.; Dwyer, R. M.; Kerin, M. J.; Smith, T. J., Amplification-free detection of microRNAs via a rapid microarray-based sandwich assay. *Analytical and bioanalytical chemistry* **2017,** *409* (14), 3497-3505.
9. Luan, J.; Seth, A.; Gupta, R.; Wang, Z.; Rathi, P.; Cao, S.; Gholami Derami, H.; Tang, R.; Xu, B.; Achilefu, S.; Morrissey, J. J.; Singamaneni, S., Ultrabright fluorescent nanoscale labels for the femtomolar detection of analytes with standard bioassays. *Nat Biomed Eng* **2020,** *4* (5), 518-530.
10. Mader, A.; Riehle, U.; Brandstetter, T.; Stickeler, E.; zur Hausen, A.; Rühe, J., Microarray-based amplification and detection of RNA by nucleic acid sequence based amplification. *Analytical and bioanalytical chemistry* **2010,** *397* (8), 3533-41.
11. Chen, K. H.; Boettiger, A. N.; Moffitt, J. R.; Wang, S.; Zhuang, X., RNA imaging. Spatially resolved, highly multiplexed RNA profiling in single cells. *Science (New York, N.Y.)* **2015,** *348* (6233), aaa6090.
12. Levsky, J. M.; Singer, R. H., Fluorescence in situ hybridization: past, present and future. *Journal of cell science* **2003,** *116* (Pt 14), 2833-8.
13. Bruch, R.; Baaske, J.; Chatelle, C.; Meirich, M.; Madlener, S.; Weber, W.; Dincer, C.; Urban, G. A., CRISPR/Cas13a-Powered Electrochemical Microfluidic Biosensor for Nucleic Acid Amplification-Free miRNA Diagnostics. *Adv Mater* **2019,** *31* (51), e1905311.
14. Chen, J. S.; Ma, E.; Harrington, L. B.; Da Costa, M.; Tian, X.; Palefsky, J. M.; Doudna, J. A., CRISPR-Cas12a target binding unleashes indiscriminate single-stranded DNase activity. *Science (New York, N.Y.)* **2018,** *360* (6387), 436-439.
15. Dai, Y.; Somoza, R. A.; Wang, L.; Welter, J. F.; Li, Y.; Caplan, A. I.; Liu, C. C., Exploring the Trans-Cleavage Activity of CRISPR-Cas12a (cpf1) for the Development of a Universal Electrochemical Biosensor. *Angewandte Chemie (International ed. in English)* **2019,** *58* (48), 17399-17405.

16. Mali, P.; Yang, L.; Esvelt, K. M.; Aach, J.; Guell, M.; DiCarlo, J. E.; Norville, J. E.; Church, G. M., RNA-guided human genome engineering via Cas9. *Science (New York, N.Y.)* **2013,** *339* (6121), 823-6.
17. Myhrvold, C.; Freije, C. A.; Gootenberg, J. S.; Abudayyeh, O. O.; Metsky, H. C.; Durbin, A. F.; Kellner, M. J.; Tan, A. L.; Paul, L. M.; Parham, L. A.; Garcia, K. F.; Barnes, K. G.; Chak, B.; Mondini, A.; Nogueira, M. L.; Isern, S.; Michael, S. F.; Lorenzana, I.; Yozwiak, N. L.; MacInnis, B. L.; Bosch, I.; Gehrke, L.; Zhang, F.; Sabeti, P. C., Field-deployable viral diagnostics using CRISPR-Cas13. *Science (New York, N.Y.)* **2018,** *360* (6387), 444-448.
18. Qin, P.; Park, M.; Alfson, K. J.; Tamhankar, M.; Carrion, R.; Patterson, J. L.; Griffiths, A.; He, Q.; Yildiz, A.; Mathies, R.; Du, K., Rapid and Fully Microfluidic Ebola Virus Detection with CRISPR-Cas13a. *ACS sensors* **2019,** *4* (4), 1048-1054.
19. Abudayyeh, O. O.; Gootenberg, J. S.; Essletzbichler, P.; Han, S.; Joung, J.; Belanto, J. J.; Verdine, V.; Cox, D. B. T.; Kellner, M. J.; Regev, A.; Lander, E. S.; Voytas, D. F.; Ting, A. Y.; Zhang, F., RNA targeting with CRISPR-Cas13. *Nature* **2017,** *550* (7675), 280-284.
20. David B. T. Cox, J. S. G., Omar O. Abudayyeh,; Brian Franklin, M. J. K., Julia Joung,Feng Zhang, RNA editing with CRISPR-Cas13. *Scinece*.
21. Jeong, Y.; Kook, Y.-M.; Lee, K.; Koh, W.-G., Metal enhanced fluorescence (MEF) for biosensors: General approaches and a review of recent developments. *Biosensors and Bioelectronics* **2018,** *111*, 102-116.
22. Luan, J.; Morrissey, J. J.; Wang, Z.; Derami, H. G.; Liu, K.-K.; Cao, S.; Jiang, Q.; Wang, C.; Kharasch, E. D.; Naik, R. R., Add-on plasmonic patch as a universal fluorescence enhancer. *Light: Science & Applications* **2018,** *7* (1), 1-13.
23. Reisch, A.; Didier, P.; Richert, L.; Oncul, S.; Arntz, Y.; Mély, Y.; Klymchenko, A. S., Collective fluorescence switching of counterion-assembled dyes in polymer nanoparticles. *Nature Communications* **2014,** *5* (1), 1-9.
24. Huang, L.; Liao, T.; Wang, J.; Ao, L.; Su, W.; Hu, J., Brilliant pitaya-type silica colloids with central–radial and high-density quantum dots incorporation for ultrasensitive fluorescence immunoassays. *Advanced Functional Materials* **2018,** *28* (4), 1705380.
25. Roth, S.; Hadass, O.; Cohen, M.; Verbarg, J.; Wilsey, J.; Danielli, A., Improving the Sensitivity of Fluorescence-Based Immunoassays by Photobleaching the Autofluorescence of Magnetic Beads. *Small (Weinheim an der Bergstrasse, Germany)* **2019,** *15* (3), e1803751.
26. Kellner, M. J.; Koob, J. G.; Gootenberg, J. S.; Abudayyeh, O. O.; Zhang, F., SHERLOCK: nucleic acid detection with CRISPR nucleases. *Nat Protoc* **2019,** *14* (10), 2986-3012.
27. Batista, P. J.; Chang, H. Y., Long noncoding RNAs: cellular address codes in development and disease. *Cell* **2013,** *152* (6), 1298-1307.
28. Congrains, A.; Kamide, K.; Oguro, R.; Yasuda, O.; Miyata, K.; Yamamoto, E.; Kawai, T.; Kusunoki, H.; Yamamoto, H.; Takeya, Y., Genetic variants at the 9p21 locus contribute to atherosclerosis through modulation of ANRIL and CDKN2A/B. *Atherosclerosis* **2012,** *220* (2), 449-455.
29. Ashraf, G. M.; Ganash, M.; Athanasios, A., Computational analysis of non-coding RNAs in Alzheimer's disease. *Bioinformation* **2019,** *15* (5), 351.
30. Mirza, A. H.; Kaur, S.; Pociot, F., Long non-coding RNAs as novel players in β cell function and type 1 diabetes. *Human genomics* **2017,** *11* (1), 17.
31. Huarte, M., The emerging role of lncRNAs in cancer. *Nature medicine* **2015,** *21* (11), 1253-61.

32. Ren, J.; Ding, L.; Zhang, D.; Shi, G.; Xu, Q.; Shen, S.; Wang, Y.; Wang, T.; Hou, Y., Carcinoma-associated fibroblasts promote the stemness and chemoresistance of colorectal cancer by transferring exosomal lncRNA H19. *Theranostics* **2018,** *8* (14), 3932-3948.
33. Vencken, S. F.; Greene, C. M.; McKiernan, P. J., Non-coding RNA as lung disease biomarkers. *Thorax* **2015,** *70* (5), 501-3.
34. Gupta, R. A.; Shah, N.; Wang, K. C.; Kim, J.; Horlings, H. M.; Wong, D. J.; Tsai, M.-C.; Hung, T.; Argani, P.; Rinn, J. L., Long non-coding RNA HOTAIR reprograms chromatin state to promote cancer metastasis. *Nature* **2010,** *464* (7291), 1071-1076.
35. Gutschner, T.; Diederichs, S., The hallmarks of cancer: a long non-coding RNA point of view. *RNA biology* **2012,** *9* (6), 703-719.
36. Brunner, A. L.; Beck, A. H.; Edris, B.; Sweeney, R. T.; Zhu, S. X.; Li, R.; Montgomery, K.; Varma, S.; Gilks, T.; Guo, X., Transcriptional profiling of long non-coding RNAs and novel transcribed regions across a diverse panel of archived human cancers. *Genome biology* **2012,** *13* (8), 1-13.
37. Gan, L.; Lv, L.; Liao, S., Long non-coding RNA H19 regulates cell growth and metastasis via the miR-22-3p/Snail1 axis in gastric cancer. *International journal of oncology* **2019,** *54* (6), 2157-2168.
38. Wang, J.; Xie, S.; Yang, J.; Xiong, H.; Jia, Y.; Zhou, Y.; Chen, Y.; Ying, X.; Chen, C.; Ye, C.; Wang, L.; Zhou, J., The long noncoding RNA H19 promotes tamoxifen resistance in breast cancer via autophagy. *Journal of hematology & oncology* **2019,** *12* (1), 81.
39. Yang, F.; Bi, J.; Xue, X.; Zheng, L.; Zhi, K.; Hua, J.; Fang, G., Up-regulated long non-coding RNA H19 contributes to proliferation of gastric cancer cells. *The FEBS journal* **2012,** *279* (17), 3159-65.
40. Chen, S.; Bu, D.; Ma, Y.; Zhu, J.; Chen, G.; Sun, L.; Zuo, S.; Li, T.; Pan, Y.; Wang, X.; Liu, Y.; Wang, P., H19 Overexpression Induces Resistance to 1,25(OH)2D3 by Targeting VDR Through miR-675-5p in Colon Cancer Cells. *Neoplasia (New York, N.Y.)* **2017,** *19* (3), 226-236.
41. Ghafouri-Fard, S.; Esmaeili, M.; Taheri, M., H19 lncRNA: Roles in tumorigenesis. *Biomedicine & pharmacotherapy = Biomedecine & pharmacotherapie* **2020,** *123*, 109774.
42. Zheng, J. F.; Guo, N. H.; Zi, F. M.; Cheng, J., Long Noncoding RNA H19 Promotes Tumorigenesis of Multiple Myeloma by Activating BRD4 Signaling by Targeting MicroRNA 152-3p. *Molecular and cellular biology* **2020,** *40* (3).
43. Chen, M. J.; Deng, J.; Chen, C.; Hu, W.; Yuan, Y. C.; Xia, Z. K., LncRNA H19 promotes epithelial mesenchymal transition and metastasis of esophageal cancer via STAT3/EZH2 axis. *The international journal of biochemistry & cell biology* **2019,** *113*, 27-36.

Supporting Information

Plasmonically-enhanced CRISPR/Cas13a-based Bioassay for Amplification-free Detection of Cancer-associated RNA

Lin Liu[1, &], Zheyu Wang[1, &], Yixuan Wang[1], Jingyi Luan[1], Jeremiah J. Morrissey[2, 3], Rajesh R. Naik[4], Srikanth Singamaneni[1, 3, *]*

Figure S1

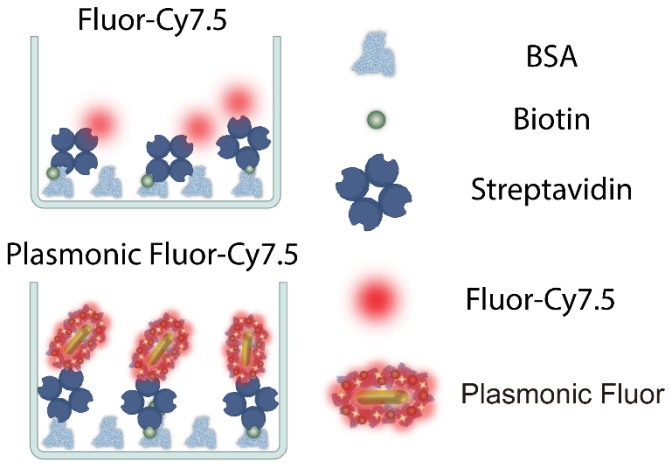

Figure S1. Schematic of the "model assay". The microtiter plate coated with BSA-biotin is exposed to streptavidin-Cy7.5 and plasmonic-fluor-Cy7.5. The fluorescence intensity corresponding to plasmonic-fluor was found to be nearly 1100-fold higher compared to that of streptavidin-Cy7.5.

Figure S2.

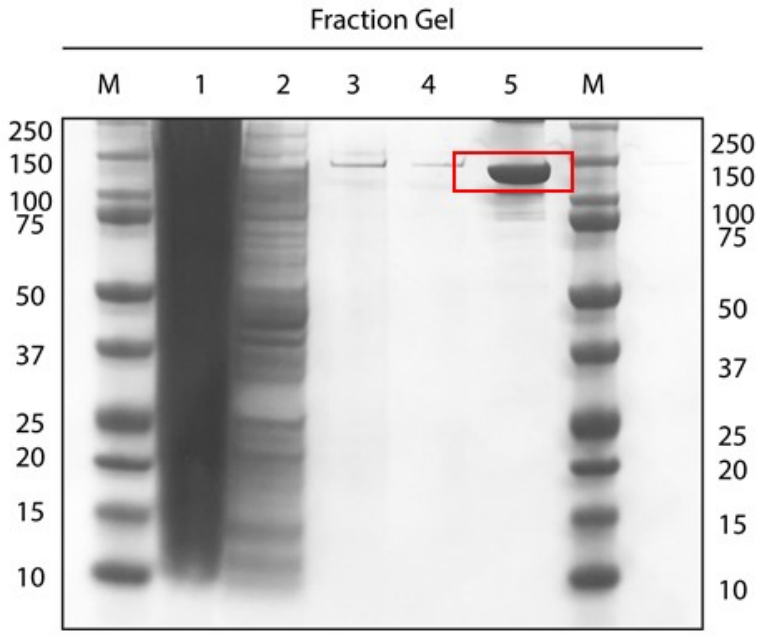

Figure S2. Coomassie-stained SDS-PAGE gel of LwaCas13a protein fraction. Different steps along the protein purification process are shown in the Coomassie-stained SDS-PAGE gel. The fractions are M, Marker; 1, cell lysate; 2, cleared cell lysate; 3, eluted fraction post SUMO protease cleavage; 4, protein solution after ion exchange chromatography; 5, final product after size-exclusion chromatography.

Figure S3

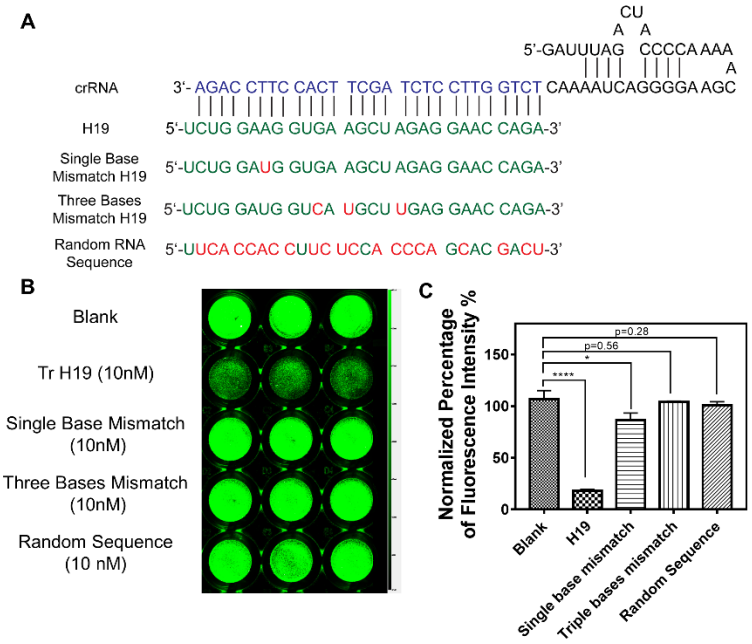

Figure S3 A) Complementary sequences of crRNA and whole RNA sequence of target and off-target (random) RNA. **B)** Fluorescence intensity map of wells corresponding to blank, target RNA, single base mismatched trRNA, three bases mismatched trRNA, and random RNA as sample, respectively. **C)** Normalized percentage of fluorescence intensity in blank sample, 10 nM target RNA, 10 nM single base mismatched trRNA, 10 nM three bases mismatched trRNA, and 10 nM random RNA. The average fluorescence intensity of blank is set as 100%. Error bars, s.d. (N =3). Data statistically significant. ****$P < 0.0001$, * $P < 0.05$ by Student t test.

Figure S4

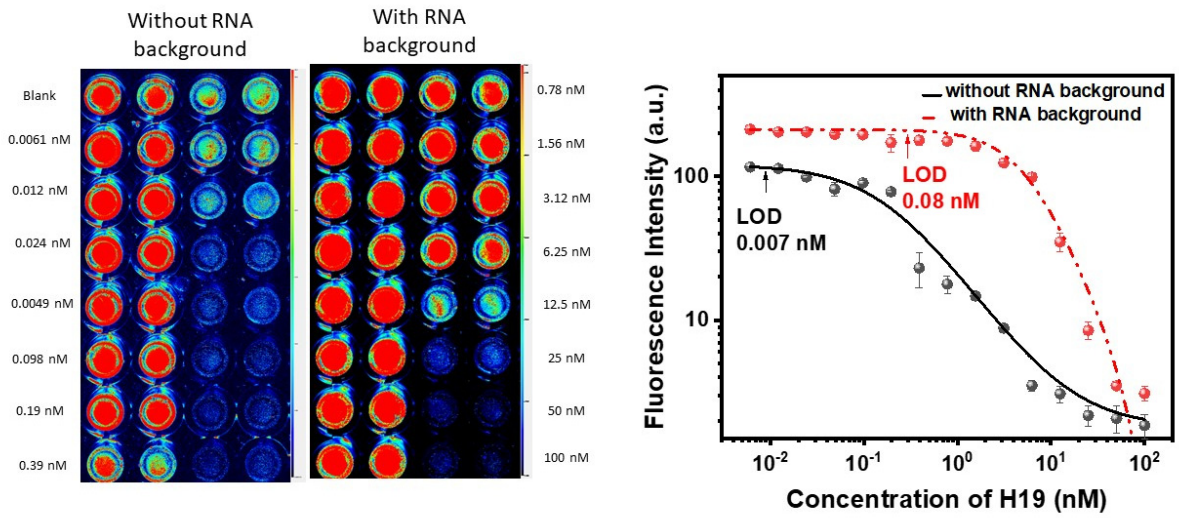

Figure S4 Left: Fluorescence images showing the dose-dependent intensity with (known concentration of target RNA spiked in 250 ng/ul total RNA extracted from 3T3 cells) and without RNA background (known concentration of target RNA spiked in reaction buffer). **Right**: Plot showing the standard curve without (black solid line) and with (red dash line) RNA background Technical replicates with n=2, and data is presented as mean $\pm$ sd..

Figure S5

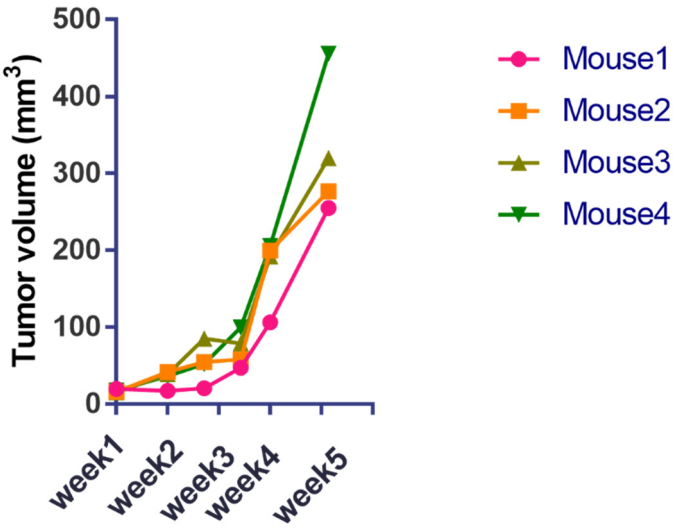

Figure S5. Plot depicting the tumor volume at different time points.

Figure S6

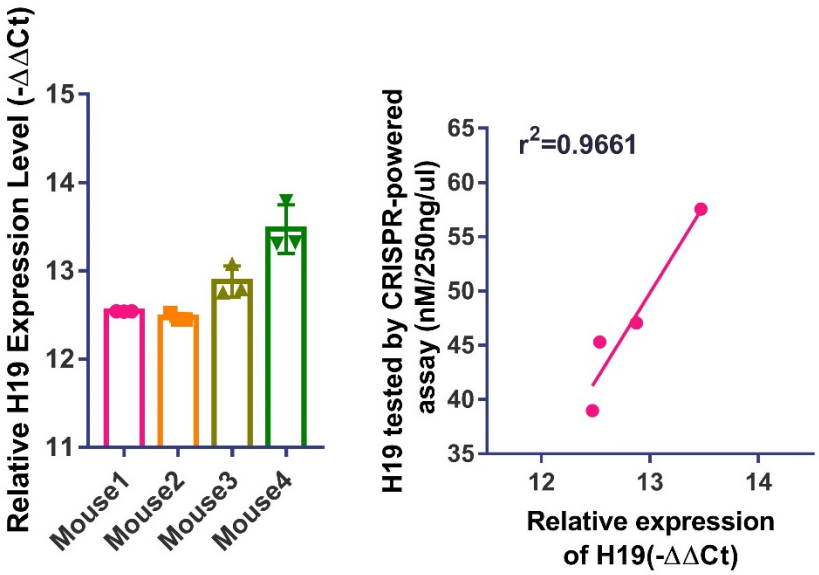

Figure S6: Left: The H19 expression in tumor tissue tested by RT-PCR. Results are shown by -ΔΔCt for different mice (1-4). Error bars, s.d. (n = 3 independent tests); Right: The correlation between H19 expression level tested by CRISPR-powered p-FLISA and RT-PCR. An r^2 of 0.9661 (Tested by Pearson r.) shows significant positive correlation between the two methods.

Figure S7

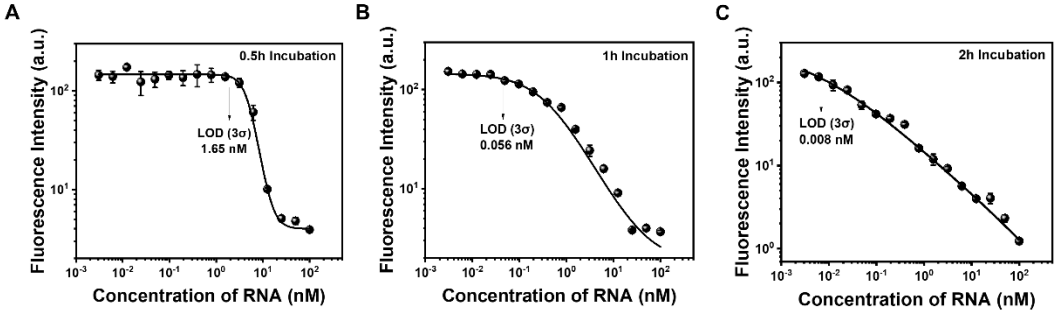

Figure S7. Effect of incubation time on LOD. **A)-C)** Plots showing the target RNA dose-dependent response of CRISPR-powered assay with different incubation times (0.5h, 1h and 2h). Technical replicates with n=2, and data is presented as mean $\pm$ sd. The LOD was found to be 1.65 nM, 0.056 nM and 0.008 nM with 0.5, 1 and 2 hours of cleavage, where better sensitivity is achieved with longer cleavage time.

Figure S8

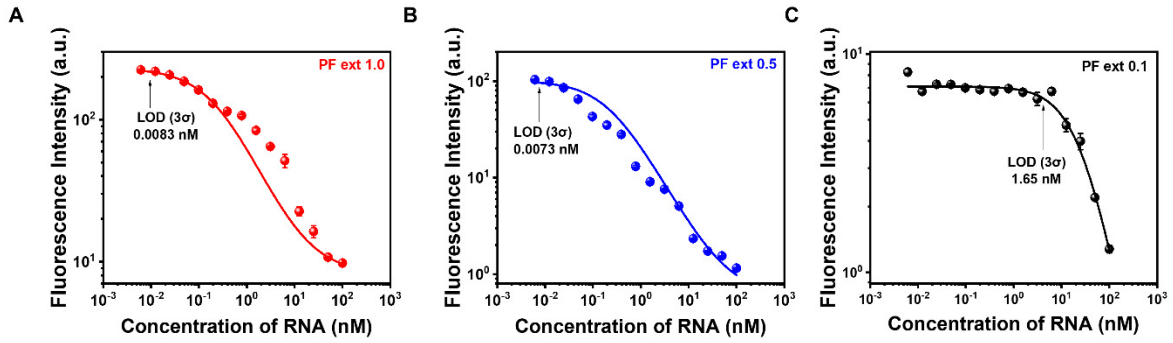

Figure S8. Effect of extinction of plasmonic-fluor on LOD. **A)-C)** Plots showing the target RNA dose-dependent response of CRISPR-powered assay with different extinction of plasmonic-fluors (ext=0.1, ext=0.5 and ext=1.0). Technical replicates with n=2, and data is presented as mean ± sd. The LOD was found to be 1.65 nM, 0.0073 nM and 0.0083 nM with ext=0.1, ext=0.5, and ext=1.0, respectively.

Supporting Table 1: Primers used in RT-PCR

Gene Name	Forward	Reverse
GAPDH	CCGGGAAACTGTGGCGTGATGG	AGGTGGAGGAGTGGGTGTCGCTGTT
H19	TCAGCTCTGGGATGATGTGGT	CTCAGGAATCGGCTCTGGAAG

Supporting Table 2: RNA and DNA used in CRISPR-powered p-FLISA assay

Name	Sequence 5'-3'
H19	UCUGGAAGGUGAAGCUAGAGGAACCAGA
crRNA	GAAAUUAAUACGACUCACUAUAGGGGAUUUAGACUACCCCA AAAACGAAGGGGACUAAAACUCUGGUUCCUCUAGCUUCACC UUCCAGA
crRNA templete	TCT GGA AGG TGA AGC TAG AGG AAC CAG A GTT TTA GTC CCC TTC GTT TTT GGG GTA GTC TAAATC CCC TATA GTG AGT CGT ATT AAT TTC
Reporter RNA	UUUUUUUUU
T7-3G Primer	GAAATTAATACGACTCACTATAGGG

Supporting Table 3:

	Reagent	Concentration and volume (per well)	Incubation time
1	Anti-FAM antibody	0.5 μg/ml in 100 μl PBS	Overnight
Three times wash with PBST			
2	BSA	1% in 300 μl PBS	1 hour
Three times wash with PBST			
3	"cleaving" 2h at 37°C		
Three times wash with PBST			
4	Product solution	100 μl	1 hour
Three times wash with PBST			
5	Plasmonic Flour	Extinction 0.5	30 minutes
Three times wash with PBST			